Metrology and microscopic picture of the integer quantum Hall effect

BY J. WEIS* AND K. VON KLITZING

Max-Planck-Institut für Festkörperforschung, Heisenbergstrasse 1, 70569 Stuttgart, Germany

Since 1990, the integer quantum Hall effect has provided the electrical resistance standard, and there has been a firm belief that the measured quantum Hall resistances are described only by fundamental physical constants—the elementary charge e and the Planck constant h. The metrological application seems not to rely on detailed knowledge of the microscopic picture of the quantum Hall effect; however, technical guidelines are recommended to confirm the quality of the sample to confirm the exactness of the measured resistance value. In this paper, we give our present understanding of the microscopic picture, derived from systematic scanning force microscopy investigations on GaAs/(AlGa)As quantum Hall samples, and relate these to the technical guidelines.

Keywords: quantum Hall effect; metrology; von Klitzing constant; contact resistance;
electronic compressibility; scanning probe microscopy

1. Introduction

The quantum Hall effect (QHE) [1] plays an important role in the discussion about units of measurements based on fundamental constants. If the technical guidelines for reliable measurements of the quantized Hall resistance are met [2], accurate and reproducible results for resistances with a relative uncertainty of a few parts in 10^9 can be obtained. A comparison between four GaAs/(AlGa)As heterostructure devices in a Wheatstone bridge even shows that the relative uncertainty for the quantized Hall resistance is smaller than 8 parts in 10^{11} [3]. Comparisons between devices from different materials, i.e. GaAs against Si [4] and GaAs against graphene [5], demonstrate that, within the experimental uncertainty of less than 3 parts in 10^9, identical resistances are observed. The Committee on Data for Science and Technology (CODATA) Task Group on Fundamental Constants concluded that there is no evidence for an inexactness of the identity between the fundamental quantized Hall resistance and the fundamental constant h/e^2 [6]. Theories of the QHE confirm that the QHE is not influenced by the gravitational field [7]; the only inexactness so far predicted comes from quantum electrodynamics, which indicate a possible radiative screening of electrical charge in a magnetic field leading to a correction at the level of 1 part in 10^{20} of magnetic fields typical for QHE experiments [8]. Such corrections are immeasurable.

*Author for correspondence (j.weis@fkf.mpg.de).

Despite the fact that the quantized Hall resistance shows a universal behaviour, the current distribution in real quantum Hall devices is complicated. For more than a decade, we have performed scanning probe measurements on a two-dimensional electron system (2DES) embedded in a GaAs/(AlGa)As heterostructure under quantum Hall conditions at temperature $T = 1.4\,\mathrm{K}$. Here we describe the role of the edges, the influence of contacts and disorder on the current distribution, and make the connections between the empirically defined guidelines for reliable QHE measurements and microscopic properties of QHE devices.

2. Some basics of the quantum Hall effect

The quantum Hall effect and its relation to fundamental physical constants were discovered in 1980 [1], and honoured by a Nobel prize in 1985:[1] the Hall resistance R_H (Hall voltage divided by applied current) measured on a two-dimensional charge carrier system (electron or hole system) at low temperatures (typically at liquid helium temperature $T = 4.2\,\mathrm{K}$) and high magnetic fields (typically several tesla) applied perpendicular to the plane of the charge carrier system shows well-defined constant values for wide magnetic field or charge carrier density variations. The values of these plateaus are perfectly described by

$$|R_\mathrm{H}| = \frac{h}{(\nu e^2)}. \tag{2.1}$$

In the original discovery in 1980, ν takes integer numbers, $i = \{1, 2, 3, 4, \ldots\}$. Later with increasing quality of the 2DES and lower temperature, for ν certain additional fractional numbers f have been discovered [10] (Nobel prize in 1998), which seem to follow $f = p/q$ with $p = \{1, 2, 3, \ldots\}$ and $q = \{3, 5, 7, \ldots\}$, with exceptions such as $f = 5/2$. The same plateau values are found by keeping the magnetic flux density B_z constant and varying the sheet electron concentration n_s. Therefore, varying the ratio n_s/B_z in certain ranges allows the Hall resistance plateaus described by equation (2.1) to be observed.

A typical Hall resistance curve versus magnetic flux density, as measured on a 2DES embedded in a GaAs/(AlGa)As heterostructure, is shown in figure 1. At low magnetic field, the Hall resistance is linearly increasing with the magnetic flux density B_z,

$$|R_\mathrm{H}| = |R_{xy}| = \left| \frac{V_y}{I_x} \right| = \left| \frac{B_z}{(-en_\mathrm{s})} \right|, \tag{2.2}$$

and allows the determination of the respective sheet charge carrier density n_s of the 2DES. At higher magnetic flux density (i.e. magnetic field) in figure 1, the Hall effect on the two-dimensional charge system shows Hall resistance values in certain magnetic field ranges, which are independent of the magnetic field. The values of these plateaus are perfectly described by equation (2.1). Such Hall resistance values are expected owing to the comparison between equations (2.2) and (2.1) only for certain well-defined ratios, $n_\mathrm{s}/B_z = \nu e/h$. The meaning of this ratio can be expressed slightly differently: taking a certain area A out of a homogeneous 2DES enclosing the integer number, $N = n_\mathrm{s}A$ of electrons, the

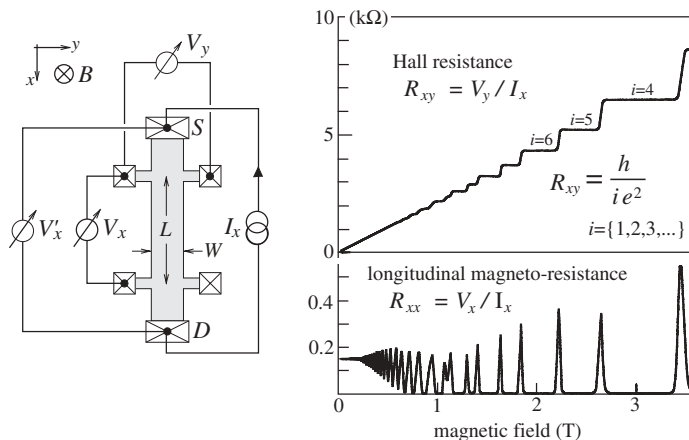[1]Historical remarks on the discovery can be found in von Klitzing [9].

Figure 1. Hall resistance curve and longitudinal magneto-resistance curve measured on a two-dimensional electron system. The Hall bar geometry and the respective electrical set-up are shown on the left.

magnetic flux penetrating this area is given by $\Phi = AB_z$. The ratio between the electron number N and the magnetic flux Φ in units of the magnetic flux quantum $\Phi_0 = e/h$ is then

$$\nu = \frac{N}{(\Phi/\Phi_0)}, \tag{2.3}$$

i.e. for each electron, ν^{-1} magnetic flux quanta are present.

Electrons in the conduction band of GaAs are nicely described as free particles with an effective mass and effective Landé g factor. The respective quantum mechanical treatment of an infinite, homogeneous, two-dimensional electron gas in high magnetic field leads to a discrete eigenenergy spectrum—the Landau levels with level spacing given by the cyclotron energy and the Zeeman energy. As the Landau level spacing and the degeneracy of each Landau level, given by $n_L = e\,B/h$, increases linearly with the magnetic field, more and more Landau levels are depopulated with increasing magnetic field, leading to a sawtooth-like shift of the chemical potential of the 2DES. This was directly visualized by using a single-electron transistor as the local electrometer on top of a 2DES embedded in a GaAs/(AlGa)As heterostructure [11–15].

For integer values of the ratio $\nu_L = n_s/n_L$, the chemical potential μ_{ch} lies between two Landau levels; therefore, at a relatively low temperature, all Landau levels below μ_{ch} are occupied, while those above μ_{ch} are unoccupied. As $\nu_L = n_s/n_L = (An_s)/(An_L) = N/(\Phi/\Phi_0) = \nu$, we can state that a quantum Hall plateau appears around the integer values of equation (2.3), which is equal to the statement that the Landau level filling factor (in short: the filling factor) ν_L of an infinite 2DES with electron density n_s has an integer value. Under this condition, the electronic system is incompressible, i.e. the chemical potential μ_{ch} jumps with increasing n_s,

$$\frac{\partial \mu_{ch}}{\partial n_s} \to \infty. \tag{2.4}$$

The absolute value of the energy gap between Landau levels is not visible in the quantum Hall resistance measurements as long as (i) the thermal energy is lower than the energy gap and (ii) the broadening of the Landau levels owing to scattering is smaller than the energy gap. The cyclotron energy gap responsible for the QHE plateau $i = 6$ at about 2.1 T in figure 1 is about one order of magnitude larger than the Zeeman energy gap responsible for the QHE plateau $i = 5$ at about 2.4 T. At magnetic fields below 1.1 T, the Zeeman gap is too small to be resolved in the QHE plateaus.

Whenever a plateau is found in the Hall resistance, the (four-terminal) longitudinal resistance $R_{xx} = V_x/I_x$ vanishes, i.e. $R_{xx} = 0$ (figure 1): the occurrence of the Hall plateau is accompanied by a dissipation-less current flowing along the sample. However, this does not mean that there is no dissipation at all. In the plateau regimes, the (two-terminal) resistance $R'_{xx} = V'_x/I_x$ measured between the current-biased contacts is approximately the same as the Hall resistance $|R_H|$, i.e. the electrical power of about $|R_H|I_x^2$ is dissipated. The heat is created in two spot-like regions, one located close to each current-biased contact [16–21]. Along the sample away from the hot spot regions, dissipation is absent, as indicated by the absence of a voltage drop along the sample. In the transition regimes between Hall plateaus, dissipation occurs along the whole sample, measurable by $R_{xx} > 0$.

The Hall plateau values with $i = 2$ and $i = 4$ are reproducible to the standard uncertainty of 10^{-9}, independent of the charge carrier density, the sample geometry and further properties of the material in which the two-dimensional charge carrier system is embedded. This is why the quantum Hall resistance has been used since 1990 as the resistance standard. The value of the quantized Hall resistance has been fixed to $R_{K\text{-}90} = 25812.807\,\Omega$ and is nowadays denoted as the conventional von Klitzing constant. Mainly GaAs–(AlGa)As–HEMT devices are used for this calibration. Devices based on graphene are now only just being explored for metrological application. Let us again emphasize the universality of the QHE: the two-dimensional charge carrier system is embedded in a crystal structure. Electrons in the conduction band of GaAs are nicely described as charged particles with an isotropic effective mass. In silicon, there exists a many valley degeneracy in the conduction band, and, in graphene, the electrons and holes behave, owing to the cone-like band structure, as mass-less Dirac particles. Obviously, these 'details' do not play any role in the measured quantum Hall plateau resistance. Only the ranges of magnetic field or density where the plateaus appear are affected. Nowadays, QHE samples are classified as a type of topological insulator [22].

To confirm the plateau values obtained on a certain sample for metrological application, the flatness of the Hall plateau, the vanishing of the longitudinal resistance $R_{xx} = 0$ and the invariance of the Hall resistance value by changing the temperature and current level are checked [2]. Increasing the quality of the samples results in the Hall plateaus becoming smaller. In consequence, a certain amount of disorder is required to obtain well-defined Hall resistance plateaus and therefore accuracy in the quantized Hall resistance value. For metrological application, the density n_s of the 2DES in a GaAs/(AlGa)As heterostructure is typically in the range of 3–$6 \times 10^{15}\,\text{m}^{-2}$ with an electron mobility of 40–$80\,\text{T}^{-1}$ and the measurements are done at temperatures around $T = 1.5\,\text{K}$ [2]. For high-precision measurements, it is desirable to have the current level as

high as possible. However, the current level is limited for the respective sample, as the QHE breaks down suddenly with increasing current beyond a certain critical current level. The typical critical sheet current density I_x/w (w is the width of the Hall bar) is of the order of 0.5–1.5 A m^{-1}. Linear and sublinear behaviours of the critical current density on sample width are observed. Also a significant increase in the working temperature degrades the Hall plateau, and the plateaus finally disappear.

Metrological applications of quantum Hall samples in Wheatstone bridges or in arrays [23]—representing other resistance values and providing higher current levels—require their use as two-terminal devices. Depending on the magnetic field orientation, the electrochemical potential of the source contact (S contact in the set-up in figure 1) is found along one edge, whereas the electrochemical potential of the drain contact (D) is found along the other edge. Without any contact resistance between the source (drain) contact and the 2DES, the applied voltage to the source and drain contacts would directly give the Hall voltage present between both edges. In this case, the two-terminal resistance would be equal to the quantum Hall resistance. However, finite contact resistances can be measured in three-terminal configurations under quantum Hall conditions in which the contact resistance is obtained from the voltage drop between the source (drain) contact and the potential probing contact that does not include a hot spot in between. Therefore, in this simple arrangement, the two-terminal resistance is not quantized. However, accurate two-terminal resistances are obtained by using the multi-connection technique [23]. To be practical, it requires contact resistances below 10 Ω for all contacts measured in the three-terminal configuration.

Since the discovery of the QHE, diverse microscopic models have been developed, sometimes emphasizing the role of either the bulk or the edges of the 2DES. Owing to the obvious effect on the plateau width, disorder and inhomogeneities in the 2DES seem to be required. In the models for the QHE, even different, sometimes contradicting, predictions about the current distribution within the 2DES under quantum Hall conditions exist. The edge state picture [24] for the integer QHE is the most popular and even presented in general textbooks. Such a picture suggests that the externally injected current flows exclusively close to the edge, which is incorrect. For more than a decade, we have performed scanning probe microscopy investigations on quantum Hall samples based on GaAs/(AlGa)As heterostructures at a temperature of 1.4 K. Our studies have examined the changes in the local electrostatic potential, i.e. we measure the difference between the local electrostatic potential with and without a current flowing through the sample— thermal equilibrium. These scan measurements directly deliver the Hall potential profile [25]. They are insensitive to any electrostatic potential variations already present in thermal equilibrium ($I_x = 0$). The properties of the GaAs/(AlGa)As heterostructures used for these experiments are very similar to the samples used in metrology, although the Hall bar mesa width has been restricted to 10–15 μm owing to the limited scan range of the scanning probe microscope (20×20 μm). In the following, we will present an outline of the main results, and focus on the role of contacts, the possible constraints for metrological applications. Details of the measurements can be found in earlier studies [25–33].

3. Measured Hall potential profiles

Figure 2 shows the Hall potential profile for different magnetic field values around a bulk Landau level filling factor of $\nu = 2$. The data are taken as y scans at x_0 in the middle of the Hall bar. In the inset of figure 2a, the quantum Hall curve around $\nu = 2$ is plotted as the reference. The given (bulk) filling factor ν is determined in these measurements via the electron density n_s obtained from low-magnetic-field Hall measurements, $\nu = n_s / n_L$. Please note that, to measure the Hall potential profiles presented in figure 2, we have applied, between the source and drain contact, an r.m.s. voltage amplitude of 20 mV, which corresponds to a current flow of about 1.5 µA for the quantum Hall plateau $\nu = 2$. We have ensured that the profiles are also obtained at lower voltage amplitudes (1 mV).

Basically three different types of Hall potential profiles can be identified [26]. (i) Coming from high magnetic field values towards the quantum Hall plateau, i.e. approaching the integer filling factor $\nu = 2$ from lower values, the Hall voltage drops linearly across the whole sample (type I). (ii) Close to the integer filling factor, at about $\nu = 1.96$, which is definitely within the quantum Hall plateau, the profile flattens at the edges and drops rather arbitrarily in the inner region of the Hall bar (type II). This is observed until $\nu = 2.09$ is reached. (iii) At $\nu = 2.14$, which is still in the quantum Hall plateau regime, the Hall voltage drop occurs at pronounced positions at the edge of the Hall bar and the profile is now flat in the inner region of the sample (type III). At a filling factor $\nu = 2.50$, the Hall voltage drops considerably linearly over the inner region, although a significant drop still occurs at the edges. Before entering the Hall plateau of $\nu = 3$, the pronounced voltage drops at the edges have disappeared and the drop is linear over the whole sample, i.e. the profile of type I is obtained again before entering the next quantum Hall plateau at lower magnetic fields.

In figure 2b, Hall potential profiles of type II are shown in comparison, taken at slightly different x positions and slightly different magnetic fields at about $\nu = 2$ [26]. As can be seen the Hall potential drops are nonlinear within the bulk region. Changing the x position for the Hall potential scan slightly by 0.2 µm, the profile is strongly modified. In addition, it is strongly affected by a small magnetic field change ($\Delta B/B = 0.5\%$). The Hall potential drop can even be non-monotonic from one edge to the other. All this hints at inhomogeneities within such samples. Based on these observations, we can state here the somehow counterintuitive result:

> Although the Hall potential distribution is strongly affected around integer values of the bulk filling factor by small magnetic field changes, the measured Hall resistance is not affected at all.

In figure 2c, the Hall potential profiles are given in colour scale for a larger magnetic field range, covering the filling factor regime $2 < \nu < 14$. As can be seen, this evolution of Hall potential profiles—from type I to type II to type III—with lowering of the magnetic field clearly repeats at each even integer filling factor $\nu > 2$, although with increasing filling factor (lower magnetic field) the evolution becomes less pronounced. Around filling factor $\nu = 3$, this evolution is also observable but to a weaker extent. This is not surprising as QHE plateaus at odd integer filling factors are given here by the Zeeman gap, whereas QHE
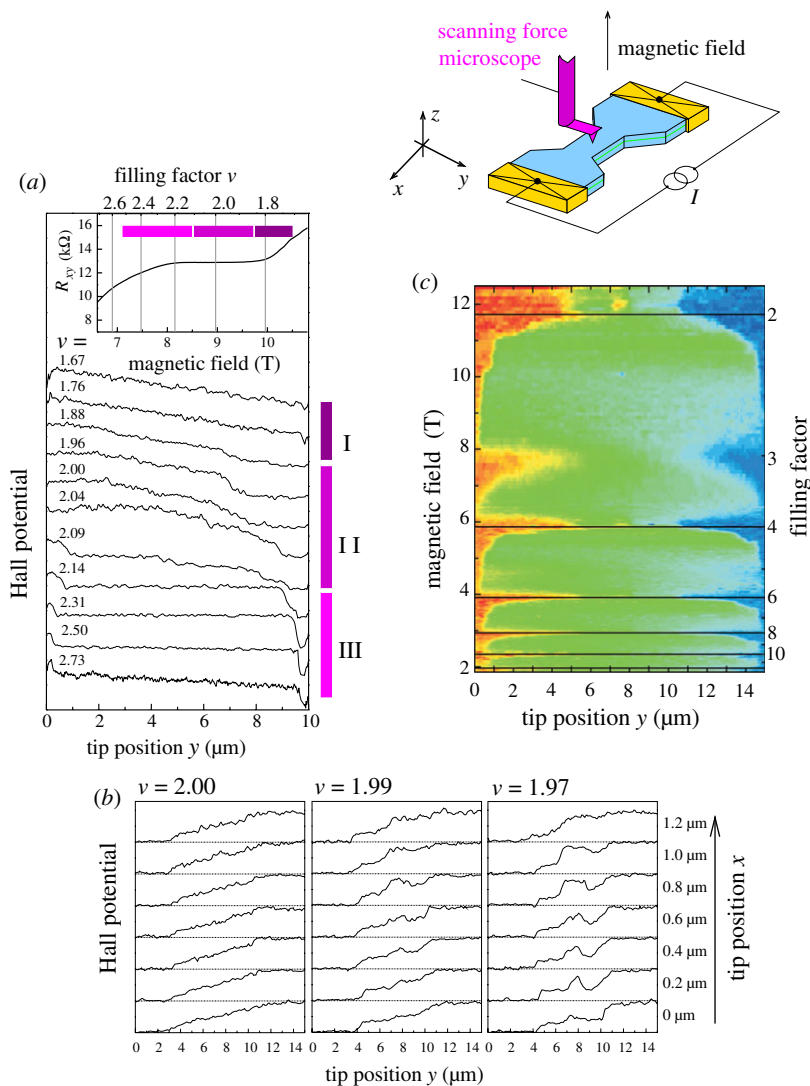
Figure 2. (*a*) Hall potential profile for different magnetic fields around filling factor $\nu = 2$ taken in the middle of the two-terminal Hall bar sample. An offset is added to each curve. Three types of Hall potential profiles are identified. Inset: Hall resistance R_{xy} around filling factor $\nu = 2$. (*b*) Hall potential profiles at slightly different scan positions and under slightly different magnetic field values close to $\nu = 2$. (*c*) Hall potential profiles in colour scale over a larger magnetic field range. Note that (*a*–*c*) were measured on different samples; however, the results are consistent.

plateaus at even filling factors are due to the cyclotron energy, which makes them less fragile against high Hall voltages (high current) and temperature.

From these observation we conclude that:

> Around integer values of the filling factor the Hall potential drops are widely spread in the bulk of the 2DES. Towards the lower magnetic field side of the quantum Hall plateau, the Hall voltage drops become more confined
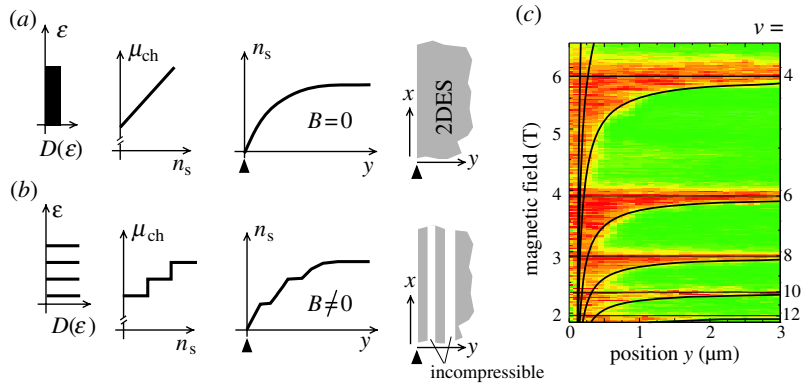
Figure 3. Sketches of density of states $D(\varepsilon)$ and chemical potential $\mu_{ch}(n_s)$ of a homogeneous two-dimensional electron gas without (a) and with (b) the applied magnetic field, leading to respective electron density profiles $n_s(y)$ at the edges of the 2DES. (c) Measured Hall potential profile (figure 2c) at one edge, compared with the expected position of the incompressible strips, given by relation (4.1).

towards the edges of the 2DES and no drop is found in the bulk. Entering the dissipative regime, i.e. leaving the quantum Hall plateau regime, the Hall voltage drop is still strongly confined to the edges; however, also in the bulk an increasing fraction of the drop is found. Before entering the regime of the next quantum Hall plateau at lower magnetic field, the drop is almost homogeneously distributed over the whole 2DES width.

This evolution of the Hall potential profile with varying ν can be related to the existence of compressible and incompressible strips running along the edges of the 2DES, predicted in several theoretical works [34–36].

4. Compressible and incompressible strips

At the edges of the 2DES, within the depletion region, the electron density n_s changes from zero to its bulk value over a typical distance of $1\,\mu m$. Within a Thomas–Fermi approximation, increasing the electron density from the edge to the bulk requires a y-dependent population of more and more electronic states. In thermodynamical equilibrium, the electron density profile $n_s(r)$ is self-consistently calculated [36] within a Thomas–Fermi approximation

  (i) by the constraint that the electrochemical potential μ_{elch}, i.e. the local chemical potential $\mu_{ch}(r)$ plus the local effective electrostatic single-electron energy $-e \cdot \phi(r)$, is constant within the whole 2DES, $\mu_{elch} = \mu_{ch}(r) - e\phi(r) = \text{const.}$; and
  (ii) by the Poisson equation that relates the local electrostatic potential $\phi(r)$ to the local electron density $n_s(r)$ by taking into account the existence of ion charges and adequate boundary conditions for $\phi(r)$ which are due to the sample;

 (iii) to self-consistently solve the electron density profile, the dependence of the chemical potential of a homogeneous 2DES on its electron density has to be known.

Without the applied magnetic field, for an idealized infinite extended 2DES, the density of states $D(\varepsilon)$ is constant versus the single-particle energy ε (figure 3a). Therefore, the chemical potential μ_{ch} increases linearly with the electron density n_s. Because of constraints (i) and (ii) discussed above, the profile $n_s(\boldsymbol{r})$ changes smoothly from the edge to the bulk as sketched in figure 3a. With a magnetic field applied perpendicularly to the plane of the 2DES, the profile is different. The density of states shows discrete degenerate Landau levels (see figure 3b) and the chemical potential increases step-like whenever an energy level is completely filled. Therefore, whenever a level is occupied, instead of requiring a large amount of chemical energy for increasing the electron concentration further towards the bulk, it is energetically favourable only to use a small amount of electrostatic energy, i.e. to keep the electron concentration constant for a region of finite width. Here, locally the 2DES is incompressible, i.e. $(\partial \mu_{ch}(\boldsymbol{r})/\partial n_s(\boldsymbol{r}))^{-1} \to 0$, the Fermi level lies between Landau levels: the electrons cannot re-arrange themselves for screening electrostatic potential variations and there is no conductivity in the direction of an electrical field. In this sense, this region behaves as an insulator. In contrast, in the adjacent compressible regions, the electrons can re-arrange at the Fermi level and therefore screen any electrostatic potential variations. Therefore, the electrostatic potential is flat in these compressible regions. As a consequence, metal-like (constant electrostatic potential) and insulator-like (constant electron concentration) strips—so-called compressible and incompressible strips, respectively—are formed in the depletion region of the 2DES [34–36].

As $\mu_{ch}(n_s)$ depends on the magnetic field, the incompressible strips shift with increasing magnetic field from the edge towards the bulk as the 'magic' filling factors appear with higher magnetic field at higher $n_s(\boldsymbol{r})$. At the same time, the incompressible strips become broader as the density gradient towards the bulk becomes smoother and the jump in $\mu_{ch}(n_s)$ becomes larger. At integer values of the bulk filling factor, the innermost incompressible strips for both edges have merged—the whole bulk is incompressible. In figure 3c, the measurements of the potential profile at the edge of the mesa for $\nu > 3$ are presented on a larger scale. For comparison, the *expected* centre positions y of the incompressible strips, i.e. the positions of even local filling factor $\mathrm{int}(\nu)$—calculated [36] for the case of thermodynamic equilibrium, i.e. without biased current—are plotted as well. The position relative to the mesa edge position y_0 is obtained from the relation

$$y - y_0 = \frac{d_0}{1 - (\mathrm{int}(\nu)/\nu)^2}, \qquad (4.1)$$

where $d_0 = 4\epsilon_0\epsilon/\pi e^2 \cdot |V_g|/n_s$ is the sample-dependent depletion width. The dielectric constant of GaAs is taken as $\epsilon \approx 13$. In our experiments, we have an etched mesa where the surface charges pinned the Fermi level at the mesa surface to the mid-gap of GaAs, and therefore here $-e\,V_g$ is taken as half of the energy gap of GaAs (1.4 eV). The agreement between the expected position and the Hall potential drop is amazingly good (solid line in figure 3c).

From the correlation between type III profiles and the expected position of incompressible strips evolving from the edge towards the bulk with increasing magnetic field, we can state that:

> Approaching a quantum Hall plateau from lower magnetic field, the Hall voltage drops mostly, then completely over the innermost incompressible strips with the local filling factor $\nu_l = \mathrm{int}(\nu)$ present at both edges of the 2DES. At integer values of the bulk filling factor, the innermost incompressible strips from both edges have merged, and the Hall potential drops over the bulk width.

Because of potential fluctuations within the bulk region of the real 2DES, the local electron density $n_s(\boldsymbol{r})$ in the bulk varies. Local electrostatic minima and maxima exist. For long-range variations, a landscape of compressible and incompressible regions is formed. Close to integer values of n_s/n_L, the bulk is mainly incompressible with compressible droplets which reshape by varying the mean sheet electron density n_s or the magnetic field B. This explains the strong dependence of the Hall potential profiles on small magnetic field variations presented in figure 2b. These inhomogeneities are also responsible for the connected incompressible bulk that exists for a finite magnetic field range.

Within the Thomas–Fermi approximation, the number of incompressible strips which can be expected in the depletion region of one edge is equal to the integer part of the bulk filling factor. However, incompressible strips become narrower the closer they are positioned to the edge, as there the confining potential becomes steeper: the Thomas–Fermi approximation breaks down, and actually these outer incompressible strips do not exist owing to the finite extension of the wave function. In our sample where the edges of the 2DES are defined by an etched mesa, we can expect—before entering a quantum Hall plateau from lower magnetic field values—at most one or two incompressible strips to exist along such edges [37]. Defining the edges of the 2DES by gate electrodes on top of the GaAs/(AlGa)As heterostructures leads at large negative voltages to a smooth edge depletion where indeed more incompressible strips are expected. The consequence of having more than one incompressible strip present at the edge will be discussed later.

5. Current distribution and quantized Hall resistance

For an infinite 2DES with applied magnetic field in the z direction and a homogeneous electric field E_y in the y direction, all Landau level states undergo a drift in the x direction, so that the local sheet current density j_x in the x direction is given by

$$j_x = \nu \frac{e^2}{h} E_y. \tag{5.1}$$

This current is flowing without dissipation as this drift is a property of the eigenfunctions solving the respective Hamiltonian. Please note that, *all* Landau levels contribute with their filling to this current density.

Actually for any smooth varying electrical field $E_y(y)$, relation (5.1) remains locally valid [38]. Integrating the sheet current density $j_x(y)$ over a certain
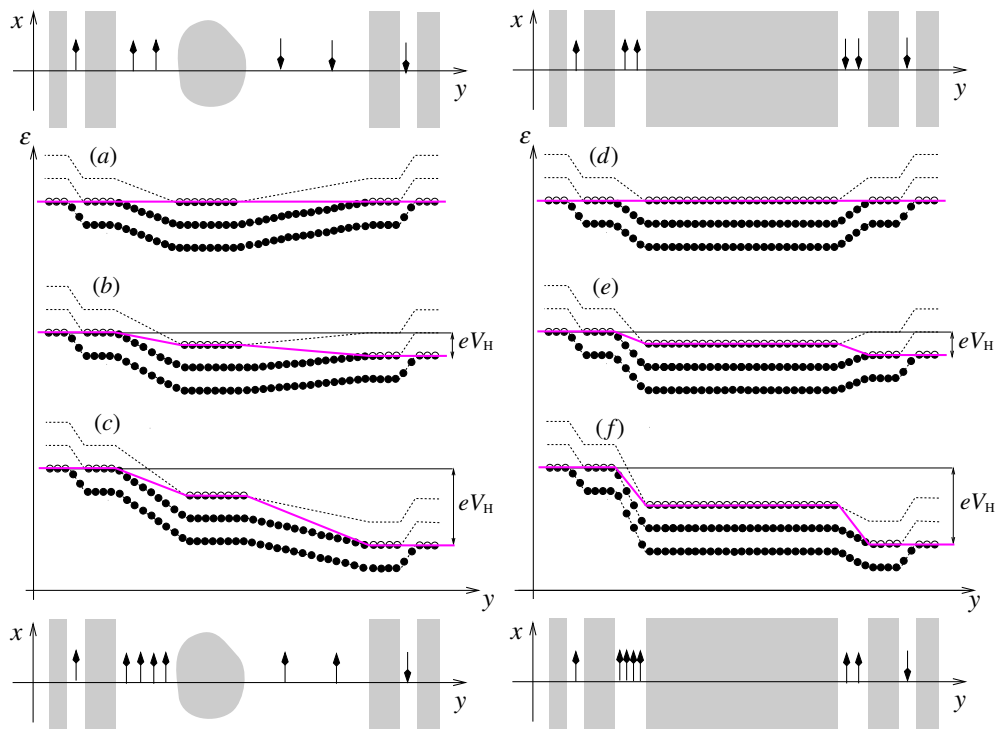
Figure 4. Sketches of Landau level bending in a cross section of the 2DES from one edge to the other edge, expected from the Hall potential profiles of type II (corresponding to $(a–c)$) and type III (corresponding to $(d–f)$) within a quantum Hall plateau. The bending is shown in (a) and (d) for thermal equilibrium, in (b) and (e) for a small Hall voltage, and in (c) and (f) for a large Hall voltage exceeding the Landau level gap energy several times. The respective Hall potential profile is shown in pink, indicating the electrochemical potential drop. On the top and at the bottom of the figure, in the (x, y) plane, the landscape of compressible (grey) and incompressible (white) regions is sketched, and the local current densities j_x driven by local electrostatic potential gradients in the y direction are indicated by arrows—at the top, for thermal equilibrium; at the bottom, for large Hall voltage.

width $y_2 - y_1$ in the y direction, where the local filling factor is constant, the integral current $\Delta I_x = \int_{y_1}^{y_2} j_x(y)\,dy$ is given by the electrostatic potential drop $\Delta \Phi_y = \int_{y_1}^{y_2} E_y(y)\,dy$ over this width,

$$\Delta I_x = \nu_l \frac{e^2}{h} \Delta \Phi_y. \tag{5.2}$$

The integral current is therefore independent of the details of the electrostatic potential drop along the path between y_1 and y_2.

Let us consider the situation around the integer value for the bulk filling factor. The bulk is mainly incompressible with the local filling factor $\nu_l = i$, with inhomogeneities embedded. Already in thermal equilibrium, i.e. equal electrochemical potential within the 2DES, the electrostatic potential varies owing to these inhomogeneities (figure 4a). Local current densities encircle the electrostatic potential minima and maxima, leading by integration within a cross section over the sample width to zero net current. This is also true for the current

densities present owing to the electrostatic potential increases towards the edges: the current densities on the left and right edges are oriented in opposite directions and compensate for each other (figure 4a (top)). As we found from our scanning probe measurements, around the integer bulk filling factor, the Hall potential drops over the bulk region of the 2DES (Hall potential profile of type II). This Hall voltage between both edges superposes locally an additional electric field in the y direction, modifying the current densities locally. As the changes are screened in compressible regions, the Hall voltage drops appear only in the incompressible regions of $\nu_l = i$. Integrated over the whole sample width, a net current

$$I_x = i\frac{e^2}{h}\,V_{\mathrm{H}} \tag{5.3}$$

is obtained. Any variations in the compressible droplet landscape affect the local current densities in the incompressible region; however, they are not visible in the integral current.

With a reduction in the magnetic field (increasing the bulk filling factor to $\nu > i$), a compressible region appears in the centre of the 2DES and the current flow is restricted to the innermost incompressible strips which move towards the two edges (profile type III with flat potential profile in the middle). The Hall potential drops approximately symmetrically over these two incompressible strips. As the measured Hall potential profile gives the change in the electrostatic potential compared with the thermal equilibrium, the externally biased current seems to be split between both edges. What happens microscopically? In figure 4d, the Landau level bending is sketched under thermal equilibrium; in figure 4e, under small Hall voltage bias V_{H}.[2] Because of this bias, the electrostatic potential drop over the innermost incompressible strip on the left-hand edge is enhanced by $\alpha\,V_{\mathrm{H}}$ ($\alpha \approx 0.5$); therefore, the dissipation-less current flowing along this incompressible strip is increased by $\Delta I_x = i\,e^2/h \cdot \alpha\,V_{\mathrm{H}}$. On the right-hand edge, the drop is diminished by $(1-\alpha)\,V_{\mathrm{H}}$ and therefore the current, flowing in the opposite direction to the left edge, is decreased by about $\Delta I_x = i\,e^2/h \cdot (1-\alpha)\,V_{\mathrm{H}}$. The electrostatic potential remains flat in the compressible regions. Integrated over the whole sample width, a net current through this cross section results from the Hall potential drops over the incompressible strips with local filling factor $\nu_l = i$; we obtain relation (5.3). At higher Hall voltage, the electrostatic potential drop on the right-hand side has reversed, and the current densities in the innermost incompressible strips on the left-hand and right-hand edges are oriented in the same direction (figure 4e (bottom)). Relation (5.3) remains valid.

In reducing the magnetic field further, these incompressible strips move further to the edges and become smaller, losing their insulating property, enhanced by local inhomogeneities. Scattering of electrons from the compressible edge into the compressible bulk and further to the opposite compressible edge becomes possible. The Hall potential drop over the innermost incompressible strips is reduced and hence so is the dissipation-less current flow. An electrochemical potential gradient

[2]A detailed description of the current distribution requires a self-consistent calculation of the local electron density under current flow [37]: the positions and widths of compressible and incompressible regions change with increasing Hall voltage, leading to asymmetrical voltage drops at both edges. It can be expected that especially the smoothness of the confining potential plays an important role in determining at which Hall voltage level the asymmetry becomes significant. For simplification, this is ignored in figure 4.

in the x direction appears, driving the electrons even in the compressible regions, which in reverse is accompanied by a Hall voltage drop within the compressible regions (profile type III with a potential drop in the middle). Because of electron scattering between the compressible edge and the bulk, the Hall resistance is no longer quantized. Before reaching the next Hall plateau at a lower magnetic field, the incompressible strips at the edges obviously have completely lost any insulating properties—they may not even exist. As a consequence, the whole width of the 2DES behaves in a compressible way and the externally biased current is more or less homogeneously distributed over the whole compressible width of the Hall bar (profile type I).

From these considerations, we can state that:

> As long as either well-pronounced incompressible strips along the edges or the connected incompressible bulk exist, they represent dissipation-less paths for a current driven as a Hall current by the electrochemical potential difference between the left and right edges.

We have found that, if the integral relation (5.3) over the sample cross section is valid, the condition of observing quantum Hall plateaus is given. However, (i) to measure the Hall voltage, it requires contacts to probe the electrochemical potentials at the edges and (ii) in the presence of more than one compressible edge strip, we have to ensure that the Hall voltage drops happen only over the innermost incompressible region, i.e. not over the incompressible strip embedded between two compressible edge strips—these compressible strips must have the same electrochemical potential.

6. Electrostatic depletion at alloyed contacts

Usually contacts to a 2DES at the edge of a 2DES are considered as an effective way of equilibrating edge and bulk [39]. The edge channel picture of Büttiker [24] assumes that one-dimensional channels along the edge are ideally transmitted into the contacts. As our measurements show, the edge state picture should not be taken literally. However, the Landauer–Büttiker formalism works rather well to phenomenologically describe the so-called adiabatic transport features. There the properties of contacts, expressed in terms of ideal and non-ideal contacts, play a crucial role.

Figure 5a shows measurements of the potential landscape close to a potential probing contact for $\nu = 2$ [28]. Obviously, the Hall potential drop drives the current through the incompressible bulk, and the contact does not affect this current distribution. Figure 5b shows the profile for the filling factor slightly above an integer value, where the bulk is mainly compressible and pronounced innermost incompressible edge strips exist; obviously, bulk and edge are on different electrochemical potentials as is the case along the etched mesa edge. Most importantly, *bulk and edge are not equilibrated in their electrochemical potentials* by the presence of the contact. This is not surprising considering that alloyed contacts and the 2DES have different work functions. Our measurements show (figure 5) that:

> For the GaAs/(AlGa)As heterostructure with low resistive NiGeAu contacts a region of *partial* depletion is formed in front of the contact edge within the

2DES which gives rise to the formation of compressible and incompressible strips along the borderline to the contact.

The innermost incompressible strip decouples—at least beyond a certain width—the bulk from the contact. Because of the electrochemical potential drop over the incompressible strip, a current is flowing without dissipation within the incompressible strip in front of the potential probing contact. It is part of the current biased into the sample. It does not pass through the contact, which would cause dissipation. The contact probes the electrochemical potential of the compressible edge at this edge position. We can state that:

> In the quantum Hall plateau regime, the externally biased current does not pass through the ohmic contacts acting as potential probes along the Hall bar edges.[3]

To emphasize, these are state-of-the-art low-resistive ohmic contacts to the 2DES. To contact the 2DES, we alloy layers of Au, Ge and Ni into our GaAs/(AlGa)As heterostructure. Systematic investigations have been performed to optimize the contact resistance between the alloyed metal and the 2DES. The materials used and the method of characterizing the contact resistances at zero magnetic field are given in the studies by Göktas *et al.* [40,41]. It turns out that the contact resistance does not depend on the area below the contact but rather on the length w of the borderline between the contact and the 2DES. Furthermore, we observe an anisotropy for the contact resistance. For a borderline between the 2DES and an alloyed metal oriented perpendicular to the [011] direction of the heterocrystal, the contact resistance R_c is lowest, whereas for borderlines perpendicular to the [01$\bar{1}$] direction, the contact resistances are higher. In the easy direction (borderline perpendicular to [011]), the specific contact resistivity value $r_c = R_c w$ is around $250\,\Omega\mu m$, corresponding to $R_c = 2.5\,\Omega$ for $w = 100\,\mu m$, and this value r_c is almost constant for all borderline lengths w ranging from 100 down to $1\,\mu m$. On the other hand, contacts defined in the hard (borderline perpendicular to [01$\bar{1}$]) direction show approximately a factor of 2 higher r_c value for a shallow-lying 2DES (about 60 nm depth) [33]; however, r_c increases for heterostructues with a deep-lying 2DES, although the amount of AuGeNi for alloying has been scaled up [40]. In addition, in the hard direction, these r_c values show a large spread and the portion of working contacts drastically decreases as the borderline becomes shorter. Therefore, the deeper the 2DES lies below the heterostructure surface, the more pronounced the anisotropy between the easy and hard directions. This anisotropy vanishes if a lower concentration of Ni is used; however, the contact resistance significantly increases. Nevertheless, the origin of anisotropy could not be clarified.

In recent systematic investigations [33]—combining scanning probe imaging with magneto-transport measurements—we demonstrated that the depletion width in front of the alloyed contacts depends—consistent with the specific contact resistivity—on the borderline orientation. Two Hall bars of the same geometry, just turned in their orientation by 90° on the same piece of

---

[3]Current flow into the contact might be due to the finite internal resistance of the voltmeter used for potential measurement.
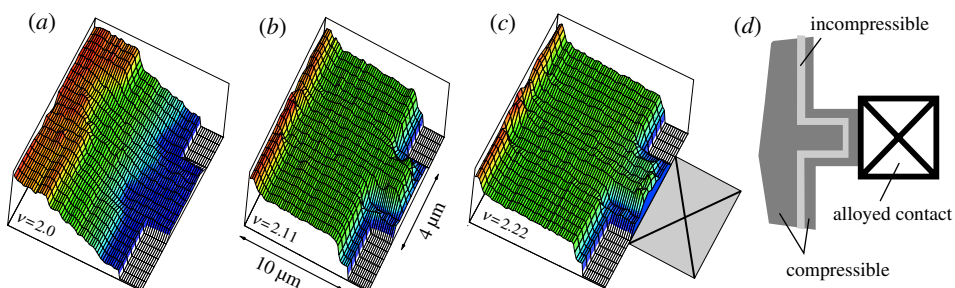
Figure 5. Hall potential profiles in the vicinity of alloyed ohmic contact for (a) $\nu = 2.0$, (b) $\nu = 2.11$ and (c) $\nu = 2.22$. The width of the Hall bar mesa is 10 μm; the width of the side arm mesa to the alloyed contact is 4 μm. The profiles (b) and (c) indicate that, in extension of an incompressible strip running along the mesa edge, the same incompressible strip is found along the interface line with the alloyed metal contact (d).
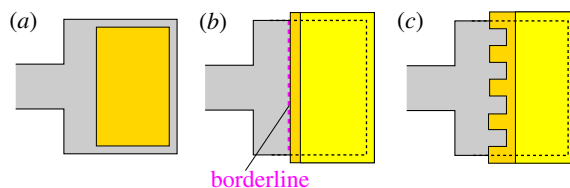

Figure 6. Bad and good geometries for alloying ohmic Au/Ge/Ni contacts in GaAs/(AlGa)As heterostructures. (a) Corbino-like contact where the alloyed metal (orange) is only in contact with a 2DES bulk but does not overlap with a mesa edge. (b) The contact resistance scales reverse linearly with the length of the borderline between the 2DES and the alloyed metal; however, this also depends on the orientation relative to the underlying heterocrystal. The Cr/Au layer (yellow), used to improve the bonding properties, must be kept behind the borderline to avoid a depletion by gating along the borderline owing to the work function difference between the 2DES and the Cr/Au layer. (c) A meander-like borderline ensures good contacts in [011] and [01$\bar{1}$] orientations.

heterostructure, show quantum Hall plateaus in different ranges of magnetic field. These and further effects are attributed to the appearance of *electrochemical potential differences between compressible edge strips running along the same edge.* Obviously—although the specific contact resistivity is only approximately a factor of 2 higher in these experiments—contacts in the hard orientation do not necessarily equilibrate these edge strips, whereas those in the easy direction do. We concluded that the extension of the partial depletion into the 2DES bulk is different for the easy and hard directions. Please note that results such as those in figure 5 were obtained for contacts in the easy direction, i.e. even contacts in the easy direction allow for a *non-equilibrium situation between a compressible edge and the compressible bulk.*

To ensure low-resistive contacts on Hall bars without taking special care regarding the Hall bar orientation, we usually design meander-like borderlines between the 2DES and the alloyed metal which contains long sections perpendicular to the [011] direction (figure 6c). Au/Ge/Ni are alloyed even beyond the border of the mesa to avoid the so-called Corbino contacts (figure 6a). Furthermore, we ensure that the layer of Cr/Au which enhances the bonding
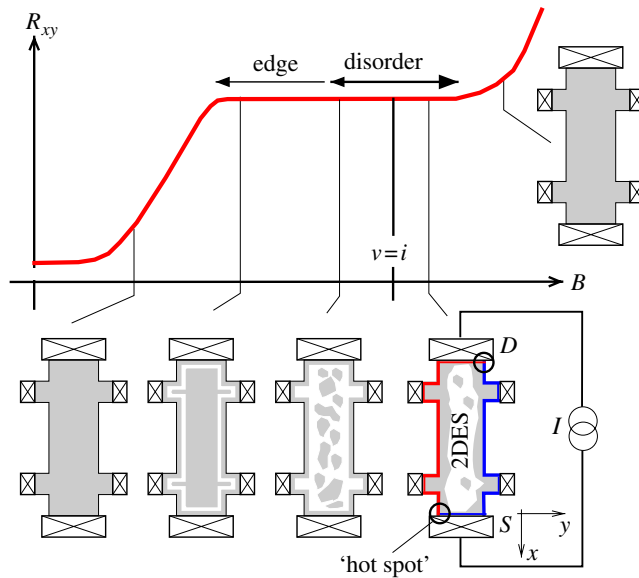
Figure 7. The evolution of the compressible and incompressible landscape at equilibrium over the regime of a quantum Hall plateau. The low magnetic field side might be enabled by the presence of well-pronounced incompressible strips along the mesa edge and in front of alloyed contacts, whereas the upper side is dominated by disorder and inhomogeneities in the 2DES bulk. The visibility of an edge-enabled quantum Hall plateau depends on the level of disorder, the level of current—these are related to the Hall bar size—as well as on the contact properties. The disorder-enabled quantum Hall plateau allows for high current levels and is most insensitive to contact properties; therefore, it is most suitable for metrological applications.

properties of the alloyed contact does not cover the heterostructure beyond the borderline of the alloyed metal to the 2DES (figure 6*b*). This would otherwise cause—owing to the workfunction difference—a depletion of the 2DES lying below.

7. Quantum Hall plateaus, contacts, metrology

Figure 7 shows schematically the evolution of the compressible and incompressible landscape within the 2DES over a quantum Hall plateau. Starting at low magnetic fields in the dissipative regime, the whole 2DES is compressible. Approaching the low magnetic field side of the quantum Hall plateau, well-pronounced incompressible strips have developed along the mesa edges and even in front of the alloyed contacts. At a certain magnetic field, the width of these incompressible strips might be able to isolate the compressible bulk from the compressible edge even under reasonably high Hall voltage drops. We are in the quantum Hall plateau regime: by applying an electrochemical potential difference between the source and the drain contact, the electrochemical potential of the source is carried by the compressible strips along one edge and the potential of drain by the compressible strips along the opposite edge into the sample. The difference is then present as a Hall voltage driving the Hall current without dissipation along

the incompressible strips on both edges through the sample. As the Hall voltage drops only over incompressible regions with the same local filling factor, relation (5.3) is valid. Entering further the quantum Hall plateau, the incompressible strips merge and the whole bulk is mainly incompressible. The Hall voltage can drop over almost the whole bulk width driving the current widely spread through the bulk in the regions of the local integer filling factor. Leaving the quantum Hall plateau at the high magnetic field side, the whole 2DES has become mainly compressible again.

This evolution of the incompressible and compressible landscape within the 2DES shows that the low and high magnetic field sides of the quantum Hall plateau might not be equal. The lower side is governed by the insulating properties of the incompressible edge strips, whereas the higher magnetic field part is dominated by the presence of inhomogeneities and disorder, stabilizing the connected incompressible bulk. In particular, the incompressible strips in front of the contacts play a crucial role whether, under the condition of a compressible bulk and pronounced incompressible edge strips, a quantum Hall plateau is observable. However, the electrostatic depletion along the 2DES edges and in front of the ohmic contacts allows a quantum Hall plateau to be obtained at even the highest quality of the 2DES, where disorder vanishes. In this sense:

> The quantum Hall effect does not necessarily require disorder to be present. The depletion at the 2DES edges and in front of the alloyed contacts might be enough.

Under high current levels, which are mandatory for metrological application of the quantum Hall effect, the Hall voltage becomes large, so that a spatially wide drop of the Hall voltage is preferable.

> Samples for metrological application have to rely on inhomogeneities (=disorder) where the Hall potential drop and the current are widely spread over the 2DES bulk. This means that the magnetic field position indicated as $\nu = i$ in figure 7 should be used for high-precision QHE experiments.

In figure 8, different scenarios for the transition region between the 2DES and the alloyed metal contact are shown. From figure 8a–c, the sample is at an integer value of the bulk filling factor. In the experimentally found case of a partial reduction of the electron concentration in front of the alloyed contact (cases (a) and (b)), the compressible strip—present in the depletion region of the 2DES along the mesa edge—is also present along the interface line to the alloyed metal. Between the metal contact and the compressible region in front of the contact, there exists a sample-dependent contact resistance which leads in the case of current flow to a voltage drop in this interface region. This contact resistance should be as small as possible; values smaller than $10\,\Omega$ are mentioned in the guidelines for quantum Hall measurements. This could be achieved by choosing respective long borderlines between the 2DES and the alloyed metal. In the (virtual) case of a flatband condition (figure 8f), the contact region between the alloyed contact and the compressible edge would be rather limited.
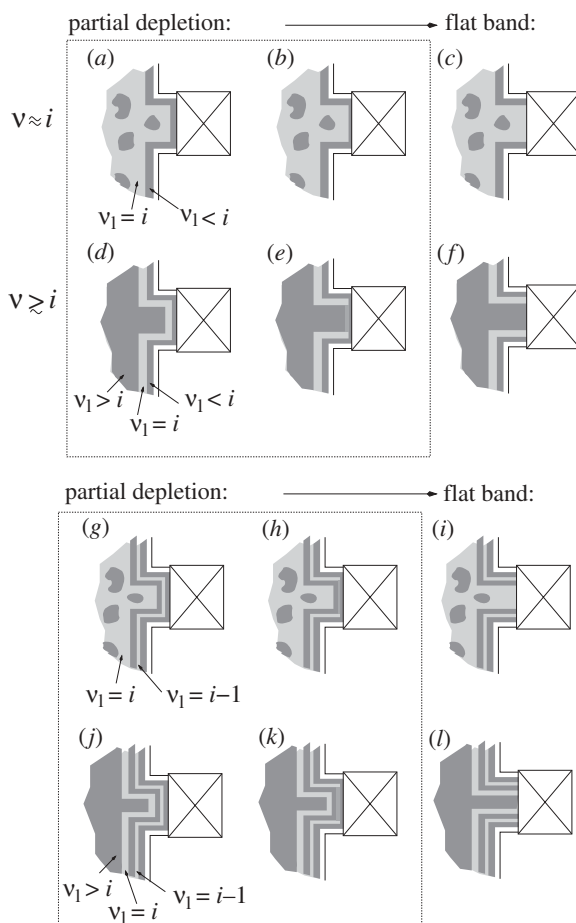
Figure 8. The compressible and incompressible landscape in the vicinity of an alloyed contact for different scenarios: for different bulk filling factors (upper and lower rows), wide and narrow depletion or flatband condition along the borderline to the contact, and the presence of one ((a)–(f)) or two ((g)–(l)) compressible edge strips.

To observe the quantum Hall plateau in the case of pronounced incompressible edge strips with a compressible bulk, a contact with a rather wide depletion region (d) is preferable. However, a long interface line between the contact and the 2DES might enhance the probability of scattering over the incompressible strip—the quantum Hall plateau gets lost. A narrow depletion (e) or even flatband condition (f) would also not allow the observation of edge-enabled quantum Hall plateaus.

What about the detailed structure of compressible and incompressible strips at the edges? A smooth confining potential along the edges of the 2DES causes the presence of some compressible and incompressible strips along the edges. In consequence, the Hall potential might drop over incompressible regions of different local filling factors. Therefore, any electrochemical potential difference between compressible edge strips has to be avoided. In this case, the contacts play a crucial role in equilibrating the compressible edge strips. Detailed comparisons

between adiabatic transport features and scanning force microscopy investigations can be found in Dahlem *et al.* [32,33]. Because of the scenarios given in figure 8*g–l*, a perfect quantum Hall plateau can be expected in case (*h*), where an equilibration happens within the rather narrow depletion region in front of the contact. A longer borderline ensures full equilibration. Under some circumstances, the situation (*k*) also allows—similar to case (*d*)—for the observation of a quantum Hall plateau.

8. Conclusion

Probing the Hall potential profiles of quantum Hall samples allows us to clarify the current distribution within such samples for the different magnetic field regimes. Theoretical work, inspired by our experiments, could reproduce the types of Hall potential profiles and predict the occurrence of quantum Hall plateaus even without localization [37].

We found at the low magnetic field side of the quantum Hall plateau that the externally biased current is confined to the pronounced innermost incompressible edge strips on both Hall bar sides, which gradually move and widen with increasing magnetic field. Finally, the Hall current is widely distributed over the mostly incompressible bulk. The quantized Hall resistances come from the fact that the Hall voltage drops over incompressible regions of same integer-valued local filling factor; the number of compressible or incompressible edge strips, resolved at the edges, does not play a role. However, in the case of a non-equilibrium situation between compressible edge strips, dissipation-less current might flow in incompressible regions of different integer-valued local filling factors—the Hall resistance quantization is lost. Furthermore, the compressible and incompressible landscape in front of the contacts and their implications for the QHE have been discussed.

As the Hall potential and current distribution are obviously related to the occurrence of incompressible regions, it is obvious that fractional quantum Hall states, being incompressible, will have a similar influence.

The application of the QHE in metrology requires the use of high current, resulting in high Hall voltage drops. They should not happen on narrow spatial widths of incompressible strips at the edge; therefore, metrological applications have to rely on the disorder and inhomogeneities in the 2DES bulk. The detailed Hall potential profile is governed by inhomogeneities within the 2DES, and also by the electrostatic environment, namely the presence of gate electrodes.

The exactness of quantum Hall plateaus relies on the contact properties, and the suppression of thermal activations and of precursors to the breakdown. We will perform further scanning probe experiments to investigate the electrically induced breakdown of the QHE. This should help to further understand and to identify weak links in respective samples for metrological applications.

References

1 von Klitzing, K., Dorda, G. & Pepper, M. 1980 New method for high-accuracy determination of the fine-structure constant based on quantized Hall resistance. *Phys. Rev. Lett.* **45**, 494–497. (doi:10.1103/PhysRevLett.45.494)

2 Delahaye, F. & Jeckelmann, B. 2003 Revised technical guidelines for reliable dc measurements of the quantized Hall resistance. *Metrologia* **40**, 217–233. (doi:10.1088/0026-1394/40/5/302)

3 Schopfer, F. & Poirier, W. 2007 Testing universality of the quantum Hall effect by means of the Wheatstone bridge. *J. Appl. Phys.* **102**, 054903. (doi:10.1063/1.2776371)

4 Hartland, A., Jones, K., Williams, J. M., Gallagher, B. L. & Galloway, T. 1991 Direct comparison of the quantized Hall resistance in gallium arsenide and silicon. *Phys. Rev. Lett.* **66**, 969–973. (doi:10.1103/PhysRevLett.66.969)

5 Tzalenchuk, A. *et al.* 2010 Towards a quantum resistance standard based on epitaxial graphene. *Nat. Nanotechnol.* **5**, 186–189. (doi:10.1038/nnano.2009.474)

6 Mohr, P. J., Taylor, B. N. & Newell, D. B. 2008 CODATA recommended values of the fundamental physical constants: 2006. *J. Phys. Chem. Ref. Data* **37**, 1187–1258.

7 Hehl, F., Obukhov, Y. N. & Rosenow, B. 2005 Is the quantum Hall effect influenced by the gravitational field? *Phys. Rev. Lett.* **93**, 096804. (doi:10.1103/PhysRevLett.93.096804)

8 Penin, A. A. 2009 Quantum Hall effect in quantum electrodynamics. *Phys. Rev. B* **79**, 113303. (doi:10.1103/PhysRevB.79.113303)

9 von Klitzing, K. 2005 Developments in the quantum Hall effect. *Phil. Trans. R. Soc. A* **363**, 2203–2219. (doi:10.1098/rsta.2005.1640)

10 Stormer, H. L., Chang, A., Tsui, D. C., Hwang, J. C. M., Gossard, A. C. & Wiegmann, W. 1983 Fractional quantization of the Hall effect. *Phys. Rev. Lett.* **50**, 1953–1956. (doi:10.1103/PhysRevLett.50.1953)

11 Wei, Y. Y., Weis, J., von Klitzing, K. & Eberl, K. 1997 Single-electron transistor as an electrometer measuring chemical potential variations. *Appl. Phys. Lett.* **71**, 2514–2517. (doi:10.1063/1.120104)

12 Wei, Y. Y., Weis, J., von Klitzing, K. & Eberl, K. 1998 Edge strips in the quantum Hall regime imaged by a single-electron transistor. *Phys. Rev. Lett.* **81**, 1674–1677. (doi:10.1103/PhysRevLett.81.1674)

13 Wei, Y. Y. 1998 Two-dimensional electron system in quantum Hall regime probed by metal single-electron transistor. PhD thesis, University of Stuttgart, Germany.

14 Weis, J., Wei, Y. Y. & von Klitzing, K. 1998 Probing the depletion region of a two-dimensional electron system in high magnetic fields. *Physica B* **256–258**, 1–7. (doi:10.1016/S0921-4526(98)00574-2)

15 Weis, J., Wei, Y. Y. & von Klitzing, K. 1998 Single-electron transistor probes two-dimensional electron system in high magnetic fields. *Physica E* **3**, 23–29. (doi:10.1016/S1386-9477(98)00214-8)

16 Klass, U., Dietsche, W., von Klitzing, K. & Ploog, K. 1991 Imaging of the dissipation in quantum-Hall-effect experiments. *Z. Phys. B* **82**, 351–354. (doi:10.1007/BF01357178)

17 Klass, U., Dietsche, W., von Klitzing, K. & Ploog, K. 1991 Fountain-pressure imaging of the dissipation in quantum-Hall experiments. *Physica B* **169**, 363–367. (doi:10.1016/0921-4526(91)90251-9)

18 Klass, U., Dietsche, W., von Klitzing, K. & Ploog, K. 1992 Image of the dissipation in gated quantum Hall effect samples. *Surf. Sci.* **263**, 97–99. (doi:10.1016/0039-6028(92)90314-V)

19 Knott, R., Dietsche, W., von Klitzing, K. & Ploog, K. 1995 Electro-optic imaging of potential distributions in the quantum Hall regime. *Semicond. Sci. Technol.* **10**, 117–126. (doi:10.1088/0268-1242/10/2/001)

20 Knott, R., Dietsche, W., von Klitzing, K. & Ploog, K. 1994 Inside a 2D electron system: images of potential and dissipation. *Solid State Electron.* **37**, 689–692. (doi:10.1016/0038-1101(94)90277-1)

21 Kawano, Y. & Komiyama, S. 2003 Spatial distribution of nonequilibrium electrons in quantum Hall devices: imaging via cyclotron emission. *Phys. Rev. B* **68**, 085328. (doi:10.1103/PhysRevB.68.085328)

22 Büttiker, M. 2009 Edge-state physics without magnetic fields. *Science* **325**, 278–279. (doi:10.1126/science.1177157)

23 Poirier, W. & Schopfer, F. 2009 Resistance metrology based on the quantum Hall effect. *Eur. Phys. J. Special Topics* **172**, 207–245. (doi:10.1140/epjst/e2009-01051-5)

24 Büttiker, M. 1988 Absence of backscattering in the quantum Hall effect in multiprobe conductors. *Phys. Rev. B* **38**, 9375–9389. (doi:10.1103/PhysRevB.38.9375)

25 Weitz, P., Ahlswede, E., Weis, J., von Klitzing, K. & Eberl, K. 2000 A low temperature scanning force microscope for investigating buried two-dimensional electron systems under quantum Hall conditions. *Appl. Surf. Sci.* **157**, 349–354. (doi:10.1016/S0169-4332(99)00550-4)

26 Weitz, P., Ahlswede, E., Weis, J., von Klitzing, K. & Eberl, K. 2000 Hall-potential investigations under quantum Hall conditions using scanning force microscopy. *Physica E* **6**, 247–250. (doi:10.1016/S1386-9477(99)00136-8)

27 Weitz, P. 1998 Untersuchungen zum Verlauf der Hall-Spannung in einem zweidimensionalen Elektronensystem unter den Bedingungen des Quanten-Hall-Effekts mittels eines Raster-Kraft-Mikroskops. PhD thesis, University of Hamburg, Germany.

28 Ahlswede, E., Weitz, P., Weis, J., Klitzing, K. v. & Eberl, K. 2001 Hall potential profiles in the quantum Hall regime measured by a scanning force microscope. *Physica B* **298**, 562–566. (doi:10.1016/S0921-4526(01)00383-0)

29 Ahlswede, E., Weis, J., von Klitzing, K. & Eberl, K. 2002 Hall potential distribution in the quantum Hall regime in the vicinity of a potential probe contact. *Physica E* **12**, 165–168. (doi:10.1016/S1386-9477(01)00267-3)

30 Ahlswede, E. 2002 Potential- und Stromverteilung beim Quanten-Hall-Effekt bestimmt mittels Rasterkraftmikroskopie. PhD thesis, University of Stuttgart, Germany.

31 Weis, J. 2006 Hall potential profiles in quantum Hall samples measured by a low-temperature scanning force microscope. *Int. J. Mod. Phys.* **21**, 1297–1306. (doi:10.1142/S0217979207042768)

32 Dahlem, F. 2008 Adiabatic transport in the quantum Hall regime: comparison between transport and scanning force microscopy investigations. PhD thesis, University of Stuttgart, Germany.

33 Dahlem, F., Ahlswede, E., Weis, J. & von Klitzing, K. 2010 Cryogenic scanning force microscopy of quantum Hall samples: adiabatic transport originating in anisotropic depletion at contact interfaces. *Phys. Rev. B* **82**, 121305. (doi:10.1103/PhysRevB.82.121305)

34 Chklovskii, D. B., Shklovskii, B. I. & Glazman, L. I. 1992 Electrostatics of edge channels. *Phys. Rev. B* **46**, 4026–4034. (doi:10.1103/PhysRevB.46.4026)

35 Chklovskii, D. B., Matveev, K. A. & Shklovskii, B. I. 1993 Ballistic conductance of interacting electrons in the quantum Hall regime. *Phys. Rev. B* **47**, 12 605–12 617. (doi:10.1103/PhysRevB.47.12605)

36 Lier, K. & Gerhardts, R. R. 1994 Self-consistent calculations of edge channels in laterally confined two-dimensional electron systems. *Phys. Rev. B* **50**, 7757–7767. (doi:10.1103/PhysRevB.50.7757)

37 Siddiki, A. & Gerhardts, R. R. 2004 Incompressible strips in dissipative Hall bars as origin of quantized Hall plateaus. *Phys. Rev. B* **70**, 195335. (doi:10.1103/PhysRevB.70.195335)

38 MacDonald, A. H., Rice, T. M. & Brinkman, W. F. 1983 Hall voltage and current distributions in an ideal two-dimensional system. *Phys. Rev. B* **28**, 3648–3650. (doi:10.1103/PhysRevB.28.3648)

39 Haug, R. J. 1993 Edge-state transport and its experimental consequences in high magnetic fields. *Semicond. Sci. Technol.* **8**, 131–153. (doi:10.1088/0268-1242/8/2/001)

40 Göktas, O., Weber, J., Weis, J. & von Klitzing, K. 2008 Alloyed ohmic contacts to two-dimensional electron system in AlGaAs/GaAs heterostructures down to submicron length scale. *Physica E* **40**, 1579–1581. (doi:10.1016/j.physe.2007.09.115)

41 Göktas, O. 2009 Small alloyed ohmic contacts to 2DES and submicron scale Corbino devices in strong magnetic fields: observation of a zero bias anomaly and single-electron charging. PhD thesis, University of Stuttgart, Germany.